Published in final edited form as:
Biochemistry. 2010 January 26; 49(3): 611–622. doi:10.1021/bi901935y.

Structure, Mechanism, and Substrate Profile for Sco3058: The Closest Bacterial Homologue to Human Renal Dipeptidase

Jennifer A. Cummings[§], **Tinh T. Nguyen**[§], **Alexander A. Fedorov**[‡], **Peter Kolb**[Ψ], **Chengfu Xu**[§], **Elena V. Fedorov**[‡], **Brian K. Shoichet**[Ψ], **David P. Barondeau**[§], **Steven C. Almo**[‡], and **Frank M. Raushel**[§,*]

[§]Department of Chemistry, P.O. Box 30012, Texas A&M University, College Station, Texas 77843

[‡]Albert Einstein College of Medicine, 1300 Morris Park Avenue, Bronx, New York 10461

[Ψ]Department of Pharmaceutical Chemistry, University of California, San Francisco, 1700 4th Street, San Francisco, California 94158-2330

Abstract

Human renal dipeptidase, an enzyme associated with glutathione metabolism and the hydrolysis of β-lactams, is similar in sequence to a cluster of ~400 microbial proteins currently annotated as nonspecific dipeptidases within the amidohydrolase superfamily. The closest homologue to the human renal dipeptidase from a fully sequenced microbe is Sco3058 from *Streptomyces coelicolor*. Dipeptide substrates of Sco3058 were identified by screening a comprehensive series of L-Xaa-L-Xaa, L-Xaa-D-Xaa and D-Xaa-L-Xaa dipeptide libraries. The substrate specificity profile shows that Sco3058 hydrolyzes a broad range of dipeptides with a marked preference for an L-amino acid at the N-terminus and a D-amino acid at the C-terminus. The best substrate identified was L-Arg-D-Asp (k_{cat}/K_m = 7.6 × 10^5 M^{-1} s^{-1}). The three-dimensional structure of Sco3058 was determined in the absence and presence of the inhibitors citrate and a phosphinate mimic of L-Ala-D-Asp. The enzyme folds as a $(\beta/\alpha)_8$-barrel and two zinc ions are bound in the active site. Site-directed mutagenesis was used to probe the importance of specific residues that have direct interactions with the substrate analogues in the active site (Asp-22, His-150, Arg-223 and Asp-320). Solvent viscosity and kinetic effects by D_2O indicate that substrate binding is relatively sticky and that proton transfers do not occurr during the rate-limiting step. A bell-shaped pH-rate profile for k_{cat} and k_{cat}/K_m indicated that one group needs to be deprotonated and a second group must be protonated for optimal turnover. Computational docking of high-energy intermediate forms of L/D-Ala-L/D-Ala to the three dimensional structure of Sco3058 identified the structural determinants for the stereochemical preferences for substrate binding and turnover.

The mammalian renal dipeptidase catalyzes the general reaction outlined in Scheme 1 (1–6). This enzyme is also able to catalyze the hydrolysis of leukotriene D_4 (2,3,7) as well as the oxidized degradation product of glutathione, L-Cys-Gly (2–4). Human renal dipeptidase (hRDP[1]) is the only enzyme in humans which has been shown to catalyze the hydrolysis of β-lactams such as SCH 29482, imipenem, meropenem and DA-1131 (8,9). However, dipeptides are consistently better substrates for hRDP than are β-lactams (2,7,10). Glycine is the preferred amino acid at the C-terminus, relative to an amino acid in the L-configuration and glycyldehydrophenylalanine is a better substrate for hRDP than glycylphenylalanine (10). With rat renal dipeptidase, L-Ala-Gly is hydrolyzed faster than L-Ala-L-Ala and Gly-D-Ala is

*To whom correspondence may be sent: (FMR) telephone: (979)-845-3373; fax: (979)-845-9452; raushel@tamu.edu.

[1]Abbreviation: hRDP, human renal dipeptidase; AHS, amidohydrolase superfamily; IPTG, isopropyl β-D-thiogalactopyranoside; PEG, polyethylene glycol.

hydrolyzed faster than Gly-L-Ala (3). Mammalian renal dipeptidases and some of their microbial homologues have been assayed with various substrates, but a complete substrate specificity profile for these types of enzymes has not been determined (2–4,6,10,11,12).

The crystal structure of hRDP has been solved with the inhibitor cilastatin bound in the active site (PDB ID: 1ITU) (13). Cilastatin is considered to be a dipeptide analog, but it does not contain a free amino group at the N-terminus and it is not hydrolyzed by hRDP. The metal center in the active site consists of two Zn ions that are bridged by a molecule from solvent (water or hydroxide) and the side chain carboxylate of Glu-125. The alpha-Zn is additionally ligated by His-20 and Asp-22 whereas the beta-Zn is coordinated to His-198 and His-219. It has been suggested that the water which bridges the two metal ions attacks the carbonyl of the peptide bond to form a tetrahedral intermediate that is stabilized by an electrostatic interaction with His-152. This residue is found at the end of β-strand 4 of the $(\beta/\alpha)_8$-barrel structure and has been shown to be important for the binding of the cilastatin inhibitor (13,14).

The structure of hRDP confirms that this enzyme is a member of the amidohydrolase superfamily (AHS). This is a rather large enzyme superfamily that has been shown to catalyze the hydrolysis of ester and amide bonds found within carbohydrate, peptide, and nucleic acid containing substrates (15). The hRDP is contained within a large cluster of proteins designated as cog2355E. This cluster of proteins is typified by an H×D motif at the end of β-strand 1 that is used to coordinate one of the two metal ions in the active site, whereas most of the other enzymes in this superfamily have an H×H motif. In hRDP the invariant aspartate at the end of β-strand 8 is not coordinated to the alpha-metal whereas in nearly all of the other members of the AHS that have been structurally characterized this residue is a direct ligand to the alpha-metal ion. The proposed chemical mechanism for the hydrolysis of dipeptides by hRDP is at variance with those mechanisms of amide bond hydrolysis proposed previously for other members of the AHS (16–18). In hRDP the carbonyl group of the amide bond about to be hydrolyzed is proposed to be polarized by an electrostatic interaction with His-152 whereas in other members of the AHS this function is contributed by a direct interaction with the beta-metal ion (13,16–18). The renal dipeptidase-like enzyme BCS-1 from *Brevibacillus borstelensis* has a tryptophan in place of the residue equivalent to His-152. BCS-1 is reported to have respectable activity ($k_{cat}/K_m = 2 \times 10^5\ M^{-1}\ s^{-1}$), which supports the conclusion that either His-152 does not play a crucial role in the chemical mechanism or that the mechanism for substrate hydrolysis of enzymes such as BCS-1 vary from that of hRDP (11).

The putative dipeptidase Sco3058 from *Streptomyces coelicolor* is the closest bacterial homologue to the human enzyme from a completely sequenced microbial organism. The sequence identity is ~41%. *S. coelicolor* is a member of soil bacteria known for their versatile metabolism and production of antibiotics and pharmaceutical agents (19). In this paper we unravel the substrate specificity of Sco3058 by determining the catalytic activity with 55 L-Xaa-L-Xaa, L-Xaa-D-Xaa and D-Xaa-L-Xaa dipeptide libraries. The results demonstrate that this enzyme is a rather promiscuous dipeptidase which is able to hydrolyze a large fraction of the ~1000 compounds screened. Nevertheless, Sco3058 showed some degree of specificity and the best substrate identified was L-Arg-D-Asp ($k_{cat}/K_m = 7.6 \times 10^5\ M^{-1}\ s^{-1}$). The structure of Sco3058 has been determined to a resolution of 1.3 Å in the presence and absence of dipeptide mimics. The chemical mechanism has been addressed through the utilization of pH-rate profiles, changes in solvent viscosity, and the utilization of site directed mutants.

Materials and Methods

Materials

All chemicals were obtained from Sigma Aldrich, unless otherwise stated. The coupling enzymes, glutamate-oxaloacetate transaminase and malate dehydrogenase, were purchased

from Sigma Aldrich and Calbiochem, respectively. Glycyl-D-Leu was purchased from TCI America. ICP standards were obtained from Inorganic Ventures Inc. Nitrocefin was purchased from Calbiochem. Metal analyses were conducted using inductively coupled plasma mass spectrometry (ICP-MS) as previously described (20). Oligonucleotide syntheses and DNA sequencing were performed by the Gene Technologies Lab of Texas A&M University.

Synthesis of Dipeptide Libraries

The L-Xaa-D-Xaa and L-Xaa-L-Xaa dipeptide libraries were synthesized as described previously (21,22). The 17 D-Xaa-L-Xaa libraries were synthesized in the same manner as the L-Xaa-L-Xaa libraries except that *N*-Fmoc-D-Xaa-OH amino acids were substituted for *N*-Fmoc-L-Xaa-OH amino acids. These compound libraries contain a single amino acid at the N-terminus and all of the common amino acids at the C-terminus. However, the amino acids L-Cys, D-Cys and D-Ile were not incorporated into any of the dipeptide libraries. A sample of these libraries, expected to contain ~2 nmol of each library component, was submitted for amino acid analysis (AAA) to quantify the amount of every amino acid in these libraries except for tryptophan. The amount of tryptophan in these libraries was determined by the absorbance at 280 nm.

Synthesis of Phosphinate Pseudodipeptides

Three racemic phosphinate pseudodipeptide mimics of the putative tetrahedral intermediates for the hydrolysis of Ala-Asp (**1**), Phe-Asp (**2**) and Tyr-Asp (**3**) were made as potential inhibitors of Sco3058. These compounds were synthesized according to previously described protocols (23–26). The structures of these compounds are presented in Scheme 2. For compound **1**: ^{31}P NMR (121.4 MHz, D_2O): 36.24, 36.20 ppm; MS (ESI negative mode): 238.0129 $(M-H)^-$; MS (ESI positive mode): 240.0977 $(M+H)^+$; $C_7H_{14}O_6NP$ requires 239.0559. For compound **2**: ^{31}P NMR (121.4 MHz, D_2O): 35.01 ppm; MS (ESI negative mode): 314.1116 $(M-H)^-$; MS (ESI positive mode): 316.0786 $(M+H)^+$; $C_{13}H_{18}O_6NP$ requires 315.0872. For compound **3**: ^{31}P NMR (121.4 MHz, D_2O): 34.71 ppm; MS (ESI negative mode): 330.0984 $(M-H)^-$; MS (ESI positive mode): 332.0828 $(M+H)^+$; $C_{13}H_{18}O_7NP$ requires 331.0821.

Cloning and Expression of Sco3058

The gene for Sco3058 (gi| 21221500) was amplified from *Streptomyces coelicolor* A3(2) genomic DNA with the primers 5'-GCAGGAGCCATATGACATCGCTGGAGAAGGCCCGCGAGCTGCTGCGC-3' and 5'-CGCGGAATTCAGCCTTCCGGCTGCTCGGCGGCCGTGCCG-3'. The *Pfx* platinum polymerase (Invitrogen), 0.05 units/μL PCR reaction, was used according to the manufacturer's instructions except the annealing step was deleted. The PCR product was digested with *Nde*I and *EcoR*I and ligated into the pET30a(+) vector (Novagen) with T4 ligase (New England Biolabs). *E. coli* BL21 Rosetta 2 (DE3) cells were electro-transformed with the pET30a(+)−Sco3058 plasmid. Cells harboring the pET30a(+)−Sco3058 plasmid were grown at 30 °C in Terrific Broth containing 25 μg/mL and 50 μg/mL chloramphenicol and kanamycin, respectively. When the optical density at 600 nm reached ~0.6, 2.5 mM $Zn(acetate)_2$ was added and the expression of Sco3058 was induced with 1.0 mM isopropyl-β-thiogalactoside (IPTG). The cells were grown overnight at room temperature. Site-directed mutagenesis was conducted on the gene for Sco3058 at residues Asp-22, His-150, Arg-223, and Asp-320 using the QuikChange kit from Stratagene.

Purification of Sco3058

The cells containing Sco3058 were suspended in a purification buffer (20 mM Tris with 100 μg/mL phenylmethanesulfonylfluoride, pH 7.5) and lysed via sonication at 0 °C. The cell lysate was obtained by centrifugation and subsequently treated with protamine sulfate (2% w/w of

cell mass) and removed by centrifugation. The protein was precipitated at 60% ammonium sulfate (371 g/L at 0 °C), isolated by centrifugation, resuspended in 20 mM Tris, pH 7.5 and purified by size exclusion chromatography using a 3 L column of AcA34 in 20 mM Tris, pH 7.5, at a flow rate of 1.0 mL/min. The fractions containing the protein of expected size, as assessed by SDS-PAGE, were combined. Sco3058 was further purified by ion exchange chromatography with a Resource Q column (Pharmacia) using a gradient of NaCl in 50 mM Tris, pH 7.5. A final gel filtration step, with a column of Superdex 200 (Amersham Biosciences) in 50 mM HEPES, pH 7.5, was utilized to remove the salt.

Ninhydrin-Based Enzyme Assays

The measurement of dipeptidase activity was conducted in 50 mM HEPES, pH 7.5. For measurement of the inhibitory properties of the phosphinate pseudodipeptides, 0.40 mM L-Leu-D-Ala was used as the substrate and the inhibitor concentrations were varied from 0–100 μM. All assays were done at 30 °C. The formation of free amino acids was quantified using a ninhydrin-based assay as previously described (27). One volume of the enzymatic reaction was mixed with two volumes of ice-cold Cd-ninhydrin reagent (0.9 % w/v ninhydrin dissolved in 1:10:80 1 g/mL $CdCl_2$: acetic acid: EtOH), heated at 80 °C for 5 min and cooled prior to reading the absorbance at 507 nm. The correlation between the absorbance at 507 nm and the concentration of free amino acids was determined for each amino acid.

β-Lactamase Assay

Sco3058 was tested for its ability to hydrolyze the β-lactam nitrocefin. The hydrolysis of nitrocefin was monitored by the increase in absorbance at 486 nm (ε = 20,500 $M-1cm^{-1}$) in the presence of 100 mM potassium phosphate, pH 7.0. The k_{cat}/K_m was estimated by fitting the data to equation 2.

Coupled Enzyme Assays

The hydrolysis of L-Arg-L-Asp was monitored by coupling the formation of L-aspartate to the oxidation of NADH in a system that includes glutamate-oxaloacetate transaminase and malate dehydrogenase. The change in the concentration of NADH was measured spectrophotometrically using a SPECTRAmax-340 plate reader (Molecular Devices Inc.) by following the decrease in absorbance at 340 nm. The standard assay conditions contained 100 mM Tris, pH 7.5, varying concentrations of L-Arg-L-Asp, 0.36 mM NADH, 7 units of glutamate-oxaloacetate transaminase, 1.0 unit of malate dehydrogenase, 3.7 mM α-ketoglutarate, 100 mM KCl and Sco3058 in a final volume of 250 μL at 30 °C. This assay was used to determine the kinetic parameters of L-Arg-L-Asp, L-Ala-L-Asp and the K_i of citrate *vs*. the L-Arg-L-Asp substrate.

The pH-dependence of the kinetic parameters, k_{cat} and k_{cat}/K_m, was measured over the pH range of 5.5 – 10.0 at 0.25 pH intervals for the zinc-substituted enzyme. The buffers used for the pH-rate profiles were MES, BIS-TRIS, TRIS and CABS. The pH values were recorded after the completion of the assays. The effects of solvent viscosity on the activity of Sco3058 were determined at pH 7.5 using sucrose as the microviscogen at 25 °C. The concentrations of sucrose were 0%, 10%, 14%, 20%, 24%, and 32% (w/w), with corresponding η_{rel} values of 1.0, 1.3, 1.5, 1.9, 2.2, and 3.2. The solvent isotope effects on the kinetic parameters of the wild-type Sco3058 were measured in 99% D_2O at a pD of 7.90.

N-terminal Substrate Specificity of Sco3058

Dipeptide library screens were conducted in 50 mM HEPES, pH 8.0, at 30 °C. Enzyme-course studies (variable enzyme concentrations for a fixed time period) were performed by incubating 19 L-Xaa-L-Xaa, 19 L-Xaa-D-Xaa and 17 D-Xaa-L-Xaa libraries with 2-2000 nM Sco3058 for 6.5,

6.5, and 18 h, respectively. For the L-Xaa-L-Xaa and L-Xaa-D-Xaa dipeptide libraries, the absorbance at 507 nm, , was plotted as a function of Sco3058 concentration, E_t, and fit to equation 1. In the case of the D-Xaa-L-Xaa libraries, the free amino acids were quantified by measuring the absorbance at 507 nm and the linear rates of hydrolysis as a function of enzyme concentration were compared for each D-Xaa-L-Xaa library.

$$Q=A\left(1-e^{-k(\mathrm{Et})}\right) \quad (1)$$

C-terminal Substrate Specificity of Sco3058

Enzyme-course assays for six dipeptide libraries: L-Arg-L-Xaa, L-Trp-L-Xaa, L-Ala-L-Xaa, L-Met-L-Xaa, L-Arg-D-Xaa and D-Leu-L-Xaa were analyzed by HPLC for determination of the C-terminal specificity. With the exception of the D-Leu-L-Xaa library, each library was incubated at 30 °C for 5 h, with and without enzyme, in 25 mM $(NH_4)HCO_3$, pH 8.0. The D-Leu-L-Xaa library was incubated under the same conditions for 18 h. The concentrations of enzyme used were 0–1000 nM (L-Ala-L-Xaa), 0–200 nM (L-Arg-D-Xaa), 0–250 nM (L-Arg-L-Xaa, L-Trp-L-Xaa and L-Met-L-Xaa) or 20–4000 nM (D-Leu-L-Xaa). The sample preparation and data analysis were conducted as previously described (21,22).

Data Analysis

The kinetic parameters, k_{cat}, K_m, and k_{cat}/K_m, were determined by fitting the initial velocity data to equation 2 where v is the initial velocity, Et is the total enzyme concentration, k_{cat} is the turnover number, [A] is the substrate concentration, and K_m is the Michaelis constant. The profiles for the variation of k_{cat} and k_{cat}/K_m with pH were fit to equation 3, where c is the pH-independent value of y, K_a and K_b are the dissociation constants of the ionizable groups and H is the proton concentration. The kinetic constants for the inhibition of Sco3058 by the pseudodipeptide mimics were obtained by a fit of the data to equation 4 where K_i is the competitive inhibition constant.

$$v/\mathrm{E_t}=(k_{cat}\,[\mathrm{A}])/(K_m+[\mathrm{A}]) \quad (2)$$

$$\log\quad y=\log\left(c/\left(1+(\mathrm{H}/K_a)+(K_b/\mathrm{H})\right)\right) \quad (3)$$

$$v/E_t=k_{cat}\,[\mathrm{A}]/[K_m\,(1+(\mathrm{I}/K_i))+\mathrm{A}] \quad (4)$$

Crystallization and Data Collection

Crystals of Sco3058 were grown by hanging drop vapor diffusion at room temperature using 0.7–0.9 M citrate, 0.1 M imidazole, pH 8.0, and 12.0 mg/mL enzyme. Crystals were observed within 2 weeks and exhibited diffraction consistent with the space group $P3_121$, with one molecule of Sco3058 per asymmetric unit and 62% solvent. Prior to data collection, the citrate-grown crystals were transferred to a cryoprotectant solution composed of 80% mother liquor and 20% glycerol and flash-cooled and stored in liquid nitrogen. Data for the glycerol/citrate-Sco3058 were collected to a maximum resolution of 1.7 Å using the single-wavelength SSRL 7–1 beamline (Stanford Synchrotron Radiation Lightsource) and intensities were integrated and scaled with DENZO and SCALEPACK (28).

The crystals of wild type Sco3058 complexed with Zn^{2+} were grown by vapor diffusion at room temperature using the following crystallization conditions: the protein solution contained wild-type Sco3058 (14.0 mg/mL) in 50 mM HEPES, pH 7.5; the precipitant contained 22% polyacrylic acid, 0.1 M HEPES pH 7.5, and 20 mM $ZnCl_2$. Crystals appeared in 3 days and exhibited diffraction consistent with the space group $P3_121$, with one molecule of Sco3058 per asymmetric unit. Prior to data collection, the crystals were transferred to cryoprotectant solutions composed of mother liquors supplemented with 20% glycerol and flash-cooled in a nitrogen stream. Data Sco3058 with Zn were collected to 1.3 Å resolution at the NSLS X4A beamline (Brookhaven National Laboratory) on an ADSC CCD detector. Intensities were integrated and scaled with DENZO and SCALEPACK (28).

The crystals containing the Zn^{2+}-bound enzyme complex were soaked for 4 hours in cryo-buffer containing 22% polyacrylic acid, 0.1 M HEPES pH 7.5, 0.5 mM $ZnCl_2$, 30% Ethylene Glycol, and 50 mM pseudodipeptide inhibitor **1**. Crystals of the ternary complex, Sco3058·Zn^{2+}·pseudodipeptide, were flash-cooled in a nitrogen stream. Data collection and reduction for the ternary complex were analogous to the procedures used for the Sco3058·Zn^{2+} complex. The data collection statistics for all crystals are given in Table 1.

Structure Determination and Model Refinement

The Sco3058-glycerol-citrate structure was determined by molecular replacement using the program AMoRe with renal dipeptidase from human (PDB code: 1ITQ) as the template (29, 30). Manual model and solvent building were performed with Xfit and the structure was to 1.7 Å with CNS (31–33). Electron density corresponding to the bound citrate and Zn^{2+} ions was evident in the active site.

The structure of wild type Sco3058 complexed with Zn^{2+} was similarly determined by molecular replacement with PHASER (34), using the coordinates of human renal dipeptidase (pdb file 1ITQ) as the search model. Iterative cycles of automatic model rebuilding with ARP (35), manual rebuilding with TOM (36), and refinement with CNS (31) were performed. The model was refined at 1.3 Å with an R_{cryst} of 0.184 and an R_{free} of 0.198. The final structure contained protein residues 1–391, 390 water molecules and two well-defined Zn^{2+} ions. Structure determination and refinement for the ternary complex Sco3058·Zn^{2+}·pseudodipeptide were analogous to the procedures used for the Sco3058·Zn^{2+} complex. The model of the Sco3058·Zn^{2+}·pseudodipeptide complex was refined at 1.4 Å with an R_{cryst} of 0.193 and an R_{free} of 0.206. The final structure includes protein residues 1–391, 417 water molecules, two Zn^{2+} ions, and one well-defined pseudodipeptide inhibitor bound in the active site. Final crystallographic refinement statistics for all complexes are provided in Table 1.

Docking calculations

In parallel with the experimental assays, a comprehensive library of dipeptides and capped amino acids was generated computationally. This library was composed of all L-L, L-D, D-L, and D-D dipeptides as well as the *N*-acetylated, *N*-succinylated, *N*-formylated, *N*-carbamoylated, *N*-formiminoylated, and hydantoin variants of individual L- and D-amino acids. All molecules were transformed to their high-energy intermediate (HEI) forms by *in silico* reaction with a hydroxide anion. The HEI form of a potential substrate mimics the tetrahedral state of the molecule immediately after the attack of water or hydroxide (37,38). This state of a substrate should show higher complementarity towards the enzyme, as it is the form that the enzyme is pre-configured to stabilize (39). Since the reaction center is tetrahedral, two enantiomers of each HEI exist, bringing the total number of diastereomers of any given dipeptide to eight. This HEI library was docked into the binding site of Sco3058 with DOCK 3.5.54 as described previously (40). We note that the score assigned to each pose of a docked dipeptide is based

on its fit to the structure (the score consists of van der Waals and electrostatic terms and is corrected for desolvation) and does not contain any terms reflecting differences in reactivity. For a library where the reactive center is consistent, the latter term can be assumed to be approximately constant, allowing conclusions to be drawn from complentarity alone. To investigate the structural determinants for binding in more detail, the four diastereomers of the Ala-Ala dipeptide (L-L, L-D, D-L, and D-D) were analyzed separately from the rest and directly compared with the experimentally determined turnover rates.

Results

Cloning, Expression and Purification of Sco3058

The gene for Sco3058 was successfully cloned into the pET30a(+) vector. The protein was expressed at moderate levels and purified to homogeneity. The identity of Sco3058 was confirmed by sequencing the first five amino acids from the N-terminus of the purified protein. The amino acid sequence (90% MTSLE and 10% TSLEK) matched that of MTSLEK predicted from the DNA sequence for this enzyme. ICP-MS confirmed the presence of 2.0 equivalents of Zn per subunit.

N-terminal Substrate Specificity of Sco3058

The substrate specificity of Sco3058 for the amino acid at the N-terminus of the various dipeptide libraries was determined by measuring the composite rate of dipeptide hydrolysis in these libraries. A typical enzyme-course plot for the hydrolysis of the L-Arg-L-Xaa library is presented in Figure 1a. An enzyme-course plot for the slower hydrolysis of the D-Xaa-L-Xaa dipeptide libraries using D-Tyr-L-Xaa as an example is presented in Figure 1b. The relative hydrolysis rates for the L-Xaa-L-Xaa, L-Xaa-D-Xaa and D-Xaa-L-Xaa dipeptide libraries are presented in Figures 2a–c. These libraries contain a fixed amino acid at the N-terminus and 17 to 19 different amino acids at the C-terminus. For the L-Xaa-L-Xaa dipeptide libraries the N-terminal preference was for a leucine residue with slightly lower turnovers for methionine, arginine, and glutamine. For the L-Xaa-D-Xaa series of dipeptides the preference at the N-terminus is for arginine, glutamine, methionine, and leucine. With the series of D-Xaa-L-Xaa dipeptide libraries, the preferred amino acids at the N-terminus are methionine, leucine, arginine, and lysine.

C-terminal Substrate Specificity for Sco3058

The observed rates for the liberation of specific amino acids from the C-terminus of the dipeptides contained within the L-Arg-L-Xaa, L-Arg-D-Xaa, L-Ala-L-Xaa, L-Trp-L-Xaa, L-Met-L-Xaa, and D-Leu-L-Xaa are presented in Figures 3a–f, respectively. The relative rates were obtained from fits of the data to equation 1. Within each library, dipeptides that terminated with L-Asp were hydrolyzed the fastest. Proline was not detected in any of the hydrolysis products and thus dipeptides that terminate in proline are not hydrolyzed. Dipeptides with L-Val, L-Thr, L-Arg or L-Lys at the C-terminus were consistently hydrolyzed more slowly than the remaining 14 L-amino acids given the same amino acid at the N-terminus.

Kinetic Constants for Selected Substrates

The kinetic constants, k_{cat}, K_m and k_{cat}/K_m, for 25 dipeptide substrates are presented in Table 2. Of the compounds tested L-Ala-L-Asp has the highest value for k_{cat} (1400 s^{-1}) and L-Arg-D-Asp has the highest value for k_{cat}/K_m (7.6×10^5 M^{-1} s^{-1}). For the four enantiomers of the dipeptide Ala-Ala, the relative rates of hydrolysis are of the order L-Ala-D-Ala > L-Ala-L-Ala > D-Ala-D-Ala > D-Ala-L-Ala. The rates of hydrolysis of *N*-formyl-D-Glu, *N*-acetyl-D-Glu and *N*-propionyl-D-Leu at a concentration of 2.0 mM were less than 2×10^{-3} s^{-1}. Nitrocefin was slowly hydrolyzed by Sco3058 but the value of k_{cat}/K_m was less than 0.1 $M^{-1}s^{-1}$. The

phosphinate pseudodipeptide mimics **1**, **2**, and **3** were found to be competitive inhibitors of Sco3058 with K_i values of 390 ± 21 nM, 2.3 ± 0.3 μM and 1.1 ± 0.2 μM, respectively. The K_i of citrate was 25 ± 15 mM.

pH-rate profiles

The kinetic constants for the hydrolysis of the dipeptide L-Arg-L-Asp were obtained as a function of pH. The pH-rate profiles for k_{cat} and k_{cat}/K_m are presented in Figures 4a and b, respectively. The pH profiles are bell-shaped and are consistent with a single functional group that must be unprotonated for activity and another group that must be protonated for catalytic activity. The pK_a values for the effect of pH on k_{cat} (Figure 4a) were 6.2 ± 0.1 and 8.4 ± 0.1. In Figure 4b the two ionizations observed for Sco3058 are less than 2 pK_a units apart and therefore only an average of the two pK_a values of 7.6 ± 0.4 can be determined (41).

Site-directed Mutagenesis

Site-directed mutagenesis was utilized to identify residues important for enzymatic activity. Several conserved residues in the active site, including Asp-22, His-150, Arg-223, and Asp-320, were altered and the kinetic constants for the purified mutants are presented in Table 3. When Asp-22 from the H×D motif at the end of β-strand 1 was changed to histidine, no activity was detected even though the purified protein contained 2 equivalents of zinc. His-150 was mutated to asparagine and alanine, and both of these mutants exhibited a significant decrease in k_{cat} (200- and 20-fold, respectively) and the value of K_m more than doubled. The conserved Arg-223 was changed to lysine and methionine. The lysine mutant was reduced in activity by 3 orders of magnitude relative to the wild type enzyme. No hydrolytic activity was detected with the methionine mutant. The conserved Asp-320 from β-strand 8 was modified to asparagine and alanine, and no activity was observed with either mutant.

Solvent Isotope and Viscosity Effects

Solvent isotope effects were utilized to determine the effect of proton transfers during substrate turnover. The kinetic parameters were obtained for the wild type enzyme in H_2O and D_2O with L-Arg-L-Asp as the substrate. The solvent isotope effects for $^{D_2O}k_{cat}$ and $^{D_2O}(k_{cat}/K_m)$ are 1.30 ± 0.02 and 1.10 ± 0.05, respectively (data not shown). Alterations in solvent viscosity using sucrose were utilized to probe the degree of rate limitation for the binding and dissociation of products and substrates on the kinetic constants of Sco3058 (42,43). The plot of $^{o}k_{cat}/^{\eta}k_{cat}$ versus the relative solvent viscosity for the wild-type enzyme exhibits a slope of 0.05 ± 0.03 and the plot for the effect of viscosity on k_{cat}/K_m is 0.50 ± 0.05.

Structure of Sco3058

The crystal structures of Sco3058 and two additional complexes with either glycerol/citrate or the pseudodipeptide Ala-Asp inhibitor (**1**) in the active site were determined to 1.3, 1.7 and 1.4 Å, respectively. A ribbon representation of the dimeric $(\beta/\alpha)_8$-barrel structure is presented in Figure 5. The zinc in the α-site is coordinated to His-20 and Asp-22 from the H×D motif that originates from the end of β-strand 1. The zinc in the β-site is ligated to the two conserved histidines (His-191 and His-212) from the ends of β-strands 5 and 6, respectively. The two metals are bridged by Glu-123 from β-strand 3 and a hydroxide/water molecule. The next nearest water molecule to either of the two metal ions is 2.4 Å away from M_β. The conserved aspartate (Asp-320) from the end of β-strand 8 is 3.6 Å from M_α and thus does not coordinate this metal. However, this residue interacts with the bridging solvent molecule at a hydrogen bonding distance of 3.0 Å. The binuclear metal center is shown in Figure 6a.

The active site of Sco3058 in the presence of glycerol and citrate is shown in Figures 6b and 7a. In the glycerol/citrate bound structure, the α-metal is tetrahedral in coordination while the

β-metal exhibits a distorted trigonal bipyramidal geometry. In addition to the four ligands described for the native structure, the β-metal is additionally coordinated to the C3-carboxylate of citrate. This carboxylate is also ion-paired with Arg-223 and occupies the same position as the water molecule, which is 2.4 Å from M_β in the native structure. The carboxylate of citrate from the *pro*-S arm is ion-paired to His-150 while the carboxylate from the *pro*-R arm is interacting with Thr-324. The hydroxyl group attached to C3 of citrate is 2.8 Å from Asp-320 and is also hydrogen bonded with the C2 hydroxyl group of glycerol. In addition, the C1 hydroxyl group of glycerol is within hydrogen bonding distance (3.0 Å) to Asp-22 and 2.4 Å from the α-metal.

The F_o-F_c electron density map that illustrates the orientation of the pseudo dipeptide inhibitor **1** in the active site of Sco3058 is presented in Figure 8. The two chiral centers that mimic the C_α stereocenters of the N- and C-terminal ends of a dipeptide are both in the R-configuration. This would correspond to the dipeptide L-Ala-D-Asp. In this complex the β-zinc is coordinated by five ligands in a distorted trigonal bipyramidal arrangement. One of these interactions originates from the phosphinate group and another is from the carboxylate that would correspond to the C-terminal carboxylate of a dipeptide substrate. The α-metal is in a distorted square pyrimidal arrangement and the α-amino group of the inhibitor is 2.3 Å away from this metal ion. The C-terminal carboxylate of the inhibitor is ion-paired with the guanidino group of Arg-223. His-150 makes polar interactions with the phosphinate moiety at a distance of 2.7 Å. The side chain carboxylate of the inhibitor interacts with Thr-324 at a distance of 2.7 Å. The orientation of inhibitor **1** in the active site of Sco3058 is presented in Figures 6c and 7b.

Docking of Dipeptides

The docking results were post-processed to exclude all poses in which the high-energy intermediate portion of the molecule was more than 4 Å away from one of the two metal ions. The top 100 of the remaining poses were inspected visually to reject molecules with intramolecular clashes and geometries incompatible with the reaction mechanism. This left 63 molecules for further consideration. Among these, there is no clear preference for a specific residue at the N-terminus, in fact most of the 63 molecules are capped (*i.e*. *N*-acetylated, *N*-formylated, *etc*.). At the C-terminus, 41% of the amino acids are in an L-configuration, and 59% are D (no glycine residues were observed at this position). Looking at the residue types in more detail, 11% are L-glutamate, 29% are D-glutamate, 14% are L-aspartate, 21% are D-aspartate, and 3% each are L-asparagine, D-asparagine, D-serine and L-glutamine. These computed specificities, at the C-terminus, may be compared with those determined experimentally (Figure 3).

The computationally determined poses of the eight diastereomers of Ala-Ala fall into two categories based on the stereochemistry at the HEI center. Molecules with an HEI center in the *S* configuration would originate from an attack of the water molecule on the *re* face of the amide bond and those with the tetrahedral intermediate in the *R*-configuration would originate from an attack on the *si* face. In all cases, except for D-Ala-D-Ala, the intermediates corresponding to an attack from the *si* face docked in unfavorable binding modes, either forming intramolecular clashes or pointing the negatively charged oxygen (corresponding to the attacking hydroxyl) away from the catalytic zinc ions. The C-terminal carboxy moiety is always in contact with Arg-223, whereas the N-terminal amino group can form polar interactions with either the backbone carbonyl of Gly-323, the side chain of Tyr-68 or Asp-22. The proposed orientations of L-Ala-D-Ala and D-Ala-L-Ala in the active site of Sco3058 are presented in Figures 9a and b, respectively.

The overlay of the docking-derived pose of L-Ala-D-Ala with the crystallographic pose of the pseudodipeptide **1** (Figure 10) shows very good agreement in the parts that are similar. The phosphinate moiety of **1** overlaps almost perfectly with the tetrahedral HEI portion of the

dipeptide, and the C-terminal carboxy moieties both interact with Arg-223. The two backbones are lined up to a high degree, with the exception of the N-terminal amino groups, which are rotated by 90° with respect to each other.

Discussion

Substrate Specificity

The substrate specificity of Sco3058 was determined using an array of dipeptide libraries. It is evident from the data presented in Table 2 that this enzyme has the ability to hydrolyze a rather broad range of dipeptides having amino acids of either the D- or L-configuration. However, at the N-terminus, amino acids of the L-configuration are greatly preferred over those of the D-configuration. For example, the values of k_{cat}/K_m for L-Ala-D-Ala and L-Ala-L-Ala are 2–3 orders of magnitude greater than their D-Ala-D-Ala and D-Ala-L-Ala counterparts. Conversely, at the C-terminus, amino acids of the D-configuration are preferred over those of the L-configuration. Thus, the values of k_{cat}/K_m for L-Arg-D-Asp and L-Ala-D-Ala are about an order of magnitude greater than those of L-Arg-L-Asp and L-Ala-L-Ala, respectively. At the N-terminus there is a preference for arginine, methionine, glutamine, and leucine whereas at the C-terminus there is a clear preference for glutamate and aspartate. The very best substrates have k_{cat}/K_m values that exceed 10^5 M^{-1} s^{-1}. *N*-acyl derivatives of D-amino acids are hydrolyzed approximately 5 orders of magnitude more slowly than are the corresponding dipeptide substrates and thus this enzyme appears to be a true dipeptidase rather than a carboxypeptidase.

Structural Determinants of Substrate Specificity

The three dimensional structure of Sco3058 was determined in the absence of ligands and also in the presence of citrate and a pseudodipeptide analog bound in the active site. The analogue of the proposed tetrahedral intermediate was synthesized without regard for the stereochemistry at the two chiral centers. The structure of the inhibitor bound in the active site is a mimic of the dipeptide L-Ala-D-Asp. As a structural mimic of the tetrahedral addition complex, this analogue is compromised since the amide nitrogen has been substituted with a methylene group to maintain hydrolytic stability of the inhibitor. Nevertheless, the structure of this complex indicates that the free α-amino group at the N-terminus of the pseudodipeptide interacts with M_α and the side chain carboxylate of Asp-22. Conversely, the free α-carboxylate at the C-terminus interacts with M_β and the side chain guanidino group of Arg-223. The side chain carboxylate of the inhibitor interacts with Thr-324 and is in close proximity to the ε-amino group of Lys-247. The phosphinate group of the inhibitor interacts with M_β and the side chain of His-150.

A similar set of interactions is apparent in the binding of citrate in the active site of Sco3058. In many ways the structure of citrate mimics the pseudodipeptide inhibitor. Thus, the carboxylate at C3 interacts with M_β and Arg-223 in much the same way as the free α-carboxylate of the inhibitor. The carboxylate from the *pro*-R arm of citrate interacts with Thr-324 similar to how the side chain carboxylate of the inhibitor interacts with this residue. The carboxylate from the *pro*-S arm of citrate interacts with His-150 in a fashion that duplicates the interactions with the phosphinate moiety with this same residue. The closest residue to the hydroxyl group of citrate is the side chain carboxylate of Asp-320. However, there are certain interactions that are missing and this may explain why the pseudodipeptide inhibitor binds with a dissociation constant that is about 4 orders of magnitude tighter than citrate.

Docking of Dipeptides

The docking of the full spectrum of dipeptides reproduced the observed preference for D-enantiomers of the C-terminal amino acids found experimentally. Moreover, the statistics of the top 100 poses show a dominance of acidic residues at the C-terminus, consistent with

experiment. There were also discrepancies: experimentally, aspartate is preferred over glutamate, whereas the reverse is true in the docking, though in neither case were the differences large. The other residues that appear more than once in the list of 63 molecules (L-asparagine, D-asparagine, D-serine, and L-glutamine) are "true positives" in the sense that these residues are also observed with significant turnover rates in the experiments. The docking misses some of the other residues at the C-terminus that show turnover *in vitro*, such as leucine and methionine.

The interactions in the docking poses also help explain the differences in the enzyme specificities, as measured by k_{cat}/K_m, for the four Ala-Ala diastereomers. The docked poses show that if the C-terminal Ala is the L-enantiomer, its methyl group points towards Lys-247. Conversely, when this Ala is in the D-configuration, the methyl is positioned more favorably in a hydrophobic, and thus more favorable, pocket formed by Val-245 and Phe-248 (Figure 9a). This is consistent with the observed preference for a D-configuration of the C-terminal amino acid and is also borne out in the docking scores of both the L-L/L-D and D-L/D-D pairs of Ala-Ala. The variants with the C-terminal amino acid in the D-configuration receive a more favorable score. A similar rationale can be employed at the N-terminus. The most likely interactions formed by a positively charged N-terminal amino group of a dipeptide substrate are with the backbone carbonyl of Gly-323 and the sidechain of Asp-22. Under these circumstances, the sidechain of an Ala in the D-configuration would come too close to itself, forming an intramolecular clash (Figure 9b). However, the structural preference at the N-terminus is more subtle and it is likely not the only factor contributing to the observed differences in the turnover rates. This is also apparent from the overlay of the L-Ala-D-Ala dipeptide with the pseudodipeptide (**1**) in the x-ray structure where the most similar parts overlay well but the N-terminus shows the highest divergence.

Mechanism of Action

One can utilize the structure of Sco3058 in the presence of the pseudodipeptide inhibitor to propose a mode of binding for typical dipeptide substrates and a working model for the chemical mechanism of substrate activation and hydrolysis. In this model the N-terminal α-amino group of dipeptide substrates interacts with Asp-22 and M_α while the C-terminal α-carboxylate group interacts with M_β and Arg-223. The carbonyl group of the amide bond about to be hydrolyzed is polarized by M_β with assistance from His-150. Since the mutation of His-150 to an alanine reduces k_{cat} by only a factor of 20, the presence of this histidine in the active site is not critical for substrate turnover. His-150 from Sco3058 aligns with His-152 in the human renal dipeptidase. The hydrolytic water is the bridging water between the two metals (see Figure 6a). The binding of the α-carboxylate group to M_β occurs with the displacement of the non-bridging water molecule to this metal ion. The phosphinate moiety of the inhibitor mimics the addition of hydroxide to the carbonyl carbon. After attack by the bridging hydroxide on the carbonyl carbon there is a proton transfer to the side chain carboxylate of Asp-320 and a subsequent proton transfer to the leaving group amine. Asp-320 is hydrogen bonded to the bridging hydroxide and is the closest residue to the methylene group of the pseudodipeptide inhibitor and the hydroxyl at C3 of citrate. This residue is the only one in the active site that is positioned to facilitate a proton transfer from the bridging hydroxide to the leaving group amine. This mechanism is illustrated in Scheme 3 and it is very similar to those previously proposed for other members of the amidohydrolase superfamily (16–18).

Rate Limiting Steps

The reaction mechanism was also addressed with the measurement of pH-rate profiles and the effects of solvent viscosity and D_2O. The changes in the kinetic constants, k_{cat} and k_{cat}/K_m, show a bell-shaped profile. The loss of activity at low pH is consistent with the protonation of the bridging hydroxide or the carboxylate of Asp-320 that is hydrogen bonded to the bridging hydroxide. The loss of activity at high pH is more difficult to assign but it is consistent with

the deprotonation of the α-amino group of the substrate. When the reactions were conducted in D_2O there was a rather modest reduction in the value of the kinetic constants. Thus, it appears that proton transfers are not occurring during the rate limiting steps. There is, however, an effect of solvent viscosity on the value of k_{cat}/K_m. A change in solvent viscosity can modulate and diminish those steps that involve the binding and/or dissociation of substrates and products from the enzyme active site but not the chemical step (43). The value of k_{cat}/K_m is affected by the rate constants of all processes up through the first irreversible step (44). Since the value of k_{cat}/K_m is affected by solvent viscosity, it appears that the rate of substrate dissociation from the EA complex is similar in magnitude to the net rate constant for the conversion of EA to enzyme product complex, EP (43). The relatively small effect of viscosity on k_{cat} suggests that product release is not rate-limiting.

Genome Context for Sco3058 and cog2355E

The genome context of Sco3058 would not have been useful in predicting the general reaction of this protein or the substrate specificity. The neighboring protein in the genome, Sco3057, has ~40% amino acid sequence identity to Sco3058, but Sco3057 does not have a single metal-binding residue in common with Sco3058. The Sco3058 gene is also adjacent to *Pur*E (Sco3059) and *Pur*K (Sco3060) which code for proteins annotated as phosphoribosylaminoimidazole carboxylase catalytic and ATPase subunits, respectively. It is conceivable that Sco3058 could either hydrolyze a molecule such as 4-[(*N*-succinylamino) carbonyl]-5-aminoimidazole ribonucleotide (SAICAR) to liberate aspartate or supply aspartate for the SAICAR synthetase reaction through the cleavage of an Xaa-L-Asp dipeptide (45). However, the immediate proximity of *Pur*E/*Pur*K to genes which code for renal dipeptidase-like proteins is not a common feature of the genome contexts of these proteins. To the best of our knowledge, the protein encoded by the *Sir*J gene from *Leptosphaeria maculans* (gi|46403052) is the only renal dipeptidase-like protein which has been suggested to be involved in a biosynthetic pathway (46). It is unclear as to whether there is any other specific function of the microbial renal dipeptidase-like proteins beyond their ability to serve as true dipeptidases.

Conservation of Residues Within cog2355E

There are ~400 amino acid sequences from the completely sequenced bacterial genomes which are categorized as part of cog2355E. Approximately two-thirds of these sequences can be classified as renal dipeptidase-like because of the conservation of the complete set of metal ligands for the binuclear active site (13). Arginine-223 recognizes the α-carboxylate of the dipeptide, and the equivalent residue to Arg-223 is conserved in greater than 95% of the sequences found in cog2355E. Within the renal dipeptidase subset of cog2355E, the residue equivalent to His-150 in Sco3058 is semi-conserved with approximately 30% of the sequences having a histidine and 70% a tryptophan at this position. In the case of the renal dipeptidase-like protein from *Rhodobacter sphaeroides* (Rsp0802; PDB ID: 3FDG; gi|218766909) this tryptophan residue is structurally equivalent to His-150 from Sco3058 with the nitrogen of the tryptophan side chain being in the same position as the N^{ε} of the histidine. The other residues which contact or are close to citrate or the phosphinate inhibitor (*i.e*. Thr-324, Asn-151, and Lys-247) and those which are in the vicinity of the active site (e.g. Tyr-68, Val-245, and Phe-248) are not conserved among hRDP and the cluster of renal dipeptidase-like sequences. Lys-247 is actually quite rare within cog2355E. All of these residues are at the ends of or immediately follow the β-strands of the $(\beta/\alpha)_8$-barrel, which is a common location for substrate-contacting residues of AHS enzymes (16,21,22).

Given the lack of conservation of putative substrate recognition residues within the subset of human renal dipeptidase and its microbial homologues, there is an opportunity to identify enzymes with varying substrate specificities and define the structure-functional relationship

of these enzymes. Therefore, the substrate specificity profiles and the 3-dimensional structures of several microbial renal dipeptidase-like proteins are currently under investigation using the same methods applied to Sco3058.

Acknowledgments

This work was supported in part by the National Institutes of Health (GM71790), the Robert A. Welch Foundation (A-840) and the Hackerman Advanced Research Program (010366-0034-2007). PK was supported by the Swiss National Science Foundation for a Fellowship for Prospective Researchers (PBZHA-118815). The X-ray coordinates and structure factors for Sco3058 have been deposited in the Protein Data Bank (PDB accession codes: 3ID7, 3ISI, and 3K5X).

References

1. Adachi H, Tawaragi Y, Inuzuka C, Kubota I, Tsujimoto M, Nishihara T, Nakazato H. Primary Structure of Human Microsomal Dipeptidase Deduced from Molecular Cloning. J. Biol. Chem 1990;265:3992–3995. [PubMed: 2303490]
2. Adachi H, Kubota I, Okamura N, Iwata H, Tsujimoto M, Nakazato H, Nishihara T, Noguchi T. Purification and Characterization of Human Microsomal Dipeptidase. J. Biochem 1989;105:957–961. [PubMed: 2768222]
3. Kozak EM, Tate SS. Glutathione-degrading Enzymes of Microvillus Membranes. J. Biol. Chem 1982;257:6322–6327. [PubMed: 6122685]
4. McIntyre T, Curthoys NP. Renal Catabolism of Glutathione. J. Biol. Chem 1982;257:11915–11921. [PubMed: 6126478]
5. Satoh S, Keida Y, Konta Y, Maeda M, Matsumoto Y, Niwa M, Kohsaka M. Purification and molecular cloning of mouse renal dipeptidase. Biochim. Biophys. Acta 1993;1163:234–242. [PubMed: 8507661]
6. Watanabe T, Kera Y, Matsumoto T, Yamada R-H. Purification and kinetic properties of a D-amino-acid peptide hydrolyzing enzyme from pig kidney cortex and its tentative identification with renal membrane dipeptidase. Biochim. Biophys. Acta 1996;1298:109–118. [PubMed: 8948495]
7. Habib GM, Shi Z-Z, Cuevas AA, Guo Q, Matzuk MM, Lieberman MW. Leukotriene D_4 and cystinyl-bis-glycine metabolism in membrane-bound dipeptidase deficient mice. Proc. Natl. Acad. Sci. U.S.A 1998;95:4859–4863. [PubMed: 9560193]
8. Campbell BJ, Forrester LJ, Zahler WL, Burks M. β-Lactamase Activity of Purified and Partially Characterized Human Renal Dipeptidase. J. Biol. Chem 1984;259:14586–14590. [PubMed: 6334084]
9. Park SW, We JS, Kim GW, Choi SH, Park HS. Stability of New Carbapenem DA-1131 to Renal Dipeptidase (Dehydropeptidase I). Antimicrob. Agents Chemother 2002;46:575–577. [PubMed: 11796382]
10. Campbell BJ, Shih YD, Forrester LJ, Zahler WL. Specificity and inhibition studies of human renal dipeptidase. Biochim. Biophys. Acta 1988;956:110–118. [PubMed: 2844265]
11. Baek DH, Song JJ, Kwon S-J, Park C, Jung C-M, Sung MH. Characteristics of a New Enantioselective Thermostable Dipeptidase from *Brevibacillus borstelensis* BCS-1 and Its Application to Synthesis of a D-Amino-Acid-Containing Dipeptide. Appl. Environ. Microbiol 2004;70:1570–1575. [PubMed: 15006780]
12. Adachi H, Tsujimoto M. Cloning and Expression of Dipeptidase from *Acinetobacter calcoaceticus* ATCC 23055. J. Biochem 1995;118:555–561. [PubMed: 8690717]
13. Nitanai Y, Satow Y, Adachi H, Tsujimoto M. Crystal Structure of Human Renal Dipeptidase Involved in β-lactam Hydrolysis. J. Mol. Biol 2002;321:177–184. [PubMed: 12144777]
14. Keynan S, Hooper NM, Turner AJ. Identification by site-directed mutagenesis of three essential histidine residues in membrane dipeptidase, a novel mammalian zinc peptidase. Biochem. J 1997;326:47–51. [PubMed: 9337849]
15. Seibert CM, Raushel FM. Structural and Catalytic Diversity within the Amidohydrolase Superfamily. Biochemistry 2005;44:6383–6391. [PubMed: 15850372]
16. Thoden JB, Phillips GN Jr. Neal TM, Raushel FM, Holden HM. Molecular Structure of Dihydroorotase: A Paradigm for Catalysis through the Use of a Binuclear Metal Center. Biochemistry 2001;40:6989–6997. [PubMed: 11401542]

17. Marti-Arbona R, Fresquet V, Thoden JB, Davis ML, Holden HM, Raushel FM. Mechanism of the Reaction Catalyzed by Isoaspartyl Dipeptidase from *Escherichia coli*. Biochemistry 2005;44:7115–7124. [PubMed: 15882050]

18. Marti-Arbona R, Thoden JB, Holden HM, Raushel FM. Functional Significance of Glu-77 and Tyr-137 within the active site of isoaspartyl dipeptidase. Bioorg. Chem 2005;33:448–458. [PubMed: 16289685]

19. Bentley SD, Chater KF, Cerdeno-Tarraga AM, Challis GL, Thomson NR, James KD, Harris DE, Quail MA, Kieser H, Harper D, Bateman A, Brown S, Chandra G, Chen CW, Collins M, Cronin A, Fraser A, Goble A, Hidalgo J, Hornsby T, Howarth S, Huang CH, Kieser T, Larke L, Murphy L, Oliver K, O'Neil S, Rabbinowitsch E, Rajandream MA, Rutherford K, Rutter S, Seeger K, Saunders D, Sharp S, Squares R, Squares S, Taylor K, Warren T, Wietzorrek A, Woodward J, Barrell BG, Parkhill J, Hopwood DA. Complete genome sequence of the model actinomycete *Streptomyces coelicolor* A3(2). Nature 2002;417:141–147. [PubMed: 12000953]

20. Hall RS, Xiang DF, Raushel FM. *N*-Acetyl-D-glucosamine-6-phosphate Deacetylase: Substrate Activation via a Single Divalent Metal Ion. Biochemistry 2007;46:7942–7952. [PubMed: 17567047]

21. Cummings JA, Fedorov AA, Xu C, Brown S, Fedorov E, Babbitt PC, Almo SC, Raushel FM. Annotating Enzymes of Uncertain Function: The Deacylation of D-Amino Acids by Members of the Amidohydrolase Superfamily. Biochemistry 2009;48:6469–6481. [PubMed: 19518059]

22. Xiang DF, Patskovsky, Xu C, Meyer AJ, Sauder JM, Burley SK, Almo SC, Raushel FM. Functional Identification of Incorrectly Annotated Prolidases from the Amidohydrolase Superfamily of Enzymes. Biochemistry 2009;48:3730–3742. [PubMed: 19281183]

23. Buchardt J, Meldal M. Novel methodology for the solid-phase synthesis of phosphinic peptides. J. Chem. Soc., Perkin Trans 2000;1:3306–3310.

24. Georgiadis D, Matziari M, Yiotakis A. A highly efficient method for the preparation of phosphinic pseudodipeptidic blocks suitably protected for solid-phase peptide synthesis. Tetrahedron 2001;57:3471–3478.

25. Baylis EK, Campbell CD, Dingwall JG. 1-Aminoalkylphosphonous Acids. Part 1. Isosteres of the Protein Amino Acids. J. Chem. Soc., Perkin Trans 1984;1:2845–2853.

26. Liboska R, Picha J, Hanclova I, Budesinsky M, Sanda M, Jiracek J. Synthesis of methionine- and norleucine-derived phosphinopeptides. Tetrahedron Lett 2008;49:5629–5631.

27. Doi E, Shibata D, Matoba T. Modified Colorimetric Ninhydrin Methods for Peptidase Assay. Anal. Biochem 1981;118:173–184. [PubMed: 7039409]

28. Otwinowski Z, Minor W. Processing of X-ray Diffraction Data Collected in Oscillation Mode. Methods Enzymol 1997;276:307–326.

29. Baily S. The CCP4 Suite: Programs for Protein Crystallography. Acta Crystallogr. Sect. D: Biol. Crystallogr 1994;50:760–763. [PubMed: 15299374]

30. Navaza J. AMoRe: an Automated Package for Molecular Replacement. Acta Crytallogr., Sect. A: Found. Crystallogr 1994;50:157–163.

31. Brünger AT, Adams PD, Clore GM, DeLano WL, Gros P, Grosse-Kunstleve RW, Jiang JS, Kuszewski J, Nilges M, Pannu NS, Read RJ, Rice LM, Simonson T, Warren GL. Crystallography & NMR system: A New Software Suite for Macromolecular Structure Determination. Acta Crystallogr., Sect. D: Biol. Crystallogr 1998;54:905–921. [PubMed: 9757107]

32. Brunger AT. Version 1.2 of the Crystallography and NMR System. Nature Protocols 2007;2:2728–2733.

33. McRee DE. XtalView/Xfit—A Versatile Program for Manipulating Atomic Coordinates and Electron Density. J. Struct. Biol 1999;125:156–165. [PubMed: 10222271]

34. McCoy AJ, Grosse-Kunstleve RW, Storoni LC, Read RJ. Likelihood enhanced fast translation functions. Acta Crystallogr., Sect. D: Biol. Crystallogr 2005;61:458–464. [PubMed: 15805601]

35. Perrakis A, Morris R, Lamzin VS. Automated protein model building combined with iterative structure refinement. Nature Struct. Biol 1999;6:458–463. [PubMed: 10331874]

36. Jones TA. Interactive computer graphics: FRODO. Methods Enzymol 1985;115:157–171. [PubMed: 3841179]

37. Hermann JC, Ghanem E, Li Y, Raushel FM, Irwin JJ, Shoichet BK. Predicting Substrates by Docking High-Energy Intermediates to Enzyme Structures. JACS 2006;128:15882–15891.

38. Nowlan C, Li Y, Hermann JC, Evans T, Carpenter J, Ghanem E, Shoichet BK, Raushel FM. Resolution of Chiral Phosphate, Phosphonate, and Phosphinate Esters by an Enantioselective Enzyme Library. JACS 2006;128:15892–15902.

39. Hermann JC, Marti-Arbona R, Fedorov AA, Fedorov E, Fedorov E, Almo SC, Shoichet BK, Raushel FM. Structure-based activity prediction for an enzyme of unknown function. Nature 2007;448:775–779. [PubMed: 17603473]

40. Xiang DF, Kolb P, Fedorov AA, Meier MM, Fedorov LV, Nguyen TT, Sterner R, Almo SC, Shoichet BK, Raushel FM. Functional Annotation and Three-Dimensional Structure of Dr0930 from *Deinococcus radiodurans*, a Close Relative of Phosphotriesterase in the Amidohydrolase Superfamily. Biochemistry 2009;48:2237–2247. [PubMed: 19159332]

41. Cleland, WW.; Cook, PF. pH Dependence of kinetic parameters and isotope effects. In: Rogers, RL., editor. Enzyme Kinetics and Mechanism. Taylor & Francis Group; New York: 2007. p. 326-366.

42. Brouwer AC, Kirsch JF. Investigation of Diffusion-Limited Rates of Chymotrypsin Reactions by Viscosity Variation. Biochemistry 1982;21:1302–1307. [PubMed: 7074086]

43. Cleland, WW.; Cook, PF. Isotopic Probes of Kinetic Mechanism. In: Rogers, RL., editor. Enzyme Kinetics and Mechanism. Taylor & Francis Group; New York: 2007. p. 249-251.

44. Cleland WW. What Limits the Rate of an Enzyme-Catalyzed Reaction? Acc. Chem. Res 1975;8:145–151.

45. Firestine SM, Poon S-W, Mueller EJ, Stubbe J, Davisson VJ. Reactions Catalyzed by 5-Aminoimidazole Ribonucleotide Carboxylase from *Escherichia coli* and *Gallus gallus*: A Case for Divergent Catalytic Mechanisms? Biochemistry 1994;33:11927–11934. [PubMed: 7918411]

46. Gardiner DM, Cozijnsen AJ, Wilson LM, Soledade M, Pedras C, Howlett BJ. The sirodesmin biosynthetic gene cluster of the plant pathogenic fungus *Leptosphaeria maculans*. Mol. Microbiol 2004;53:1307–1318. [PubMed: 15387811]

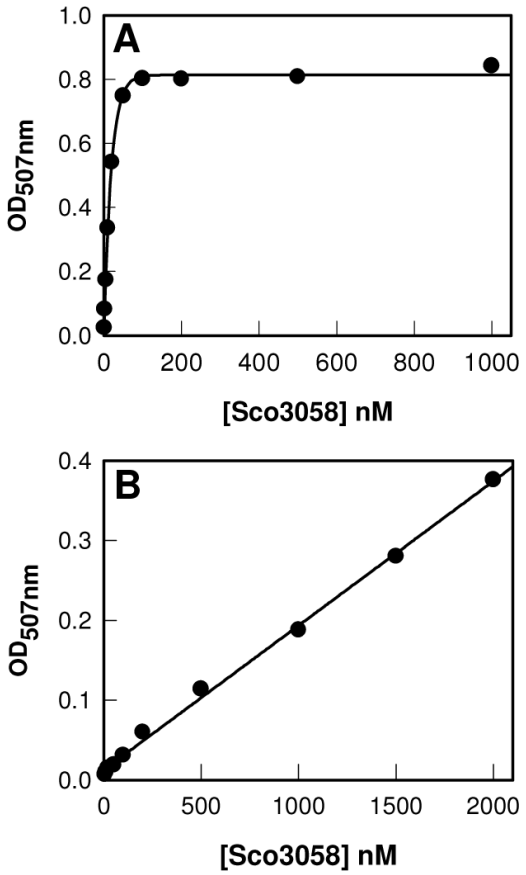

Figure 1.

Typical enzyme-course plots for the hydrolysis of dipeptide libraries. **(a)** L-Arg-L-Xaa treated with various concentrations of Sco3058. **(b)** D-Val-L-Xaa treated with various concentrations of Sco3058. Additional details are found in the text.

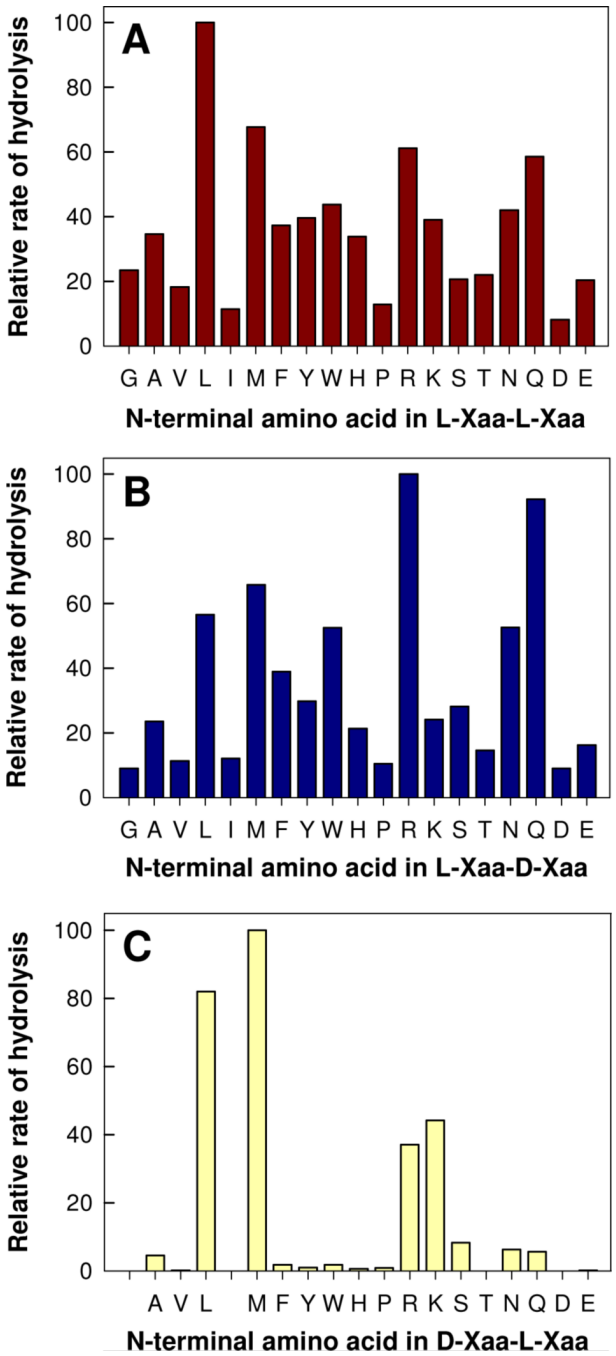

Figure 2.

N-terminal specificity for 55 dipeptide libraries. (a) Relative rates of hydrolysis for 19 L-Xaa-L-Xaa dipeptides. (b) Relative rates of hydrolysis for 19 L-Xaa-D-Xaa dipeptide libraries. (c) Relative rates of hydrolysis for 17 D-Xaa-L-Xaa dipeptide libraries.

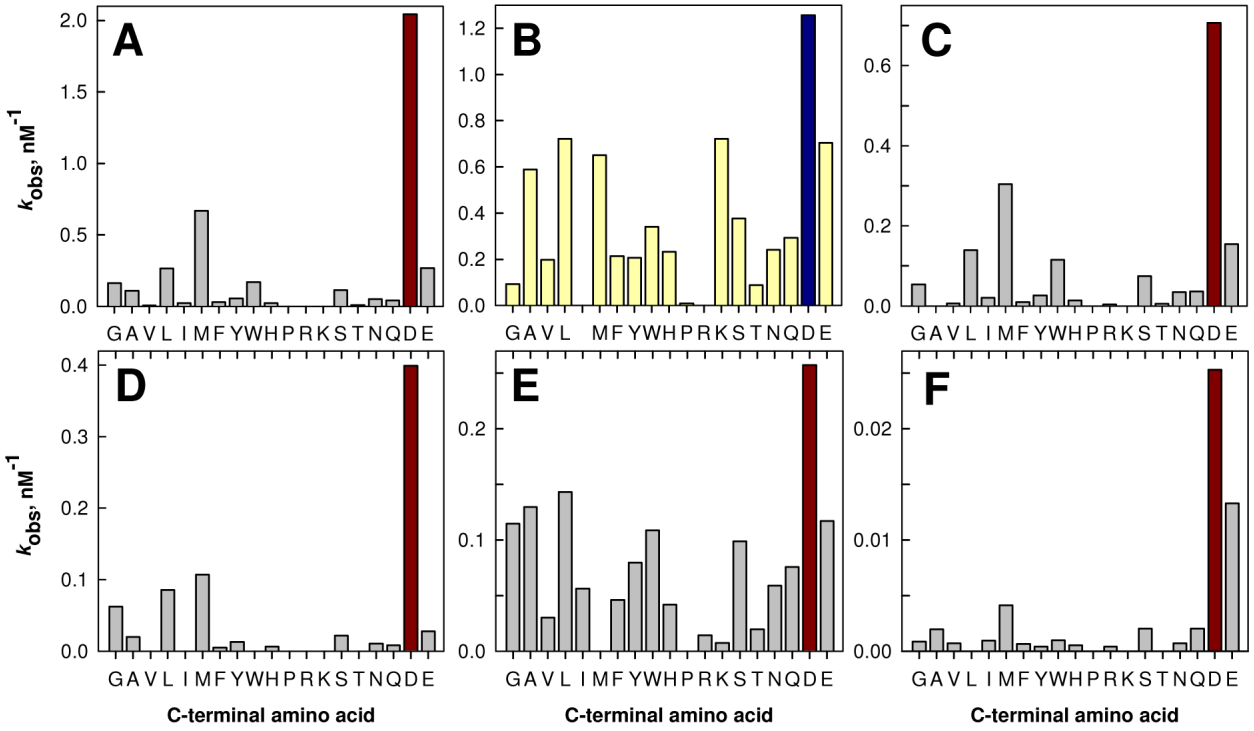

Figure 3.

C-terminal specificity for Sco3058 with six dipeptide libraries. The k_{obs} (nM^{-1}) for the hydrolysis of each dipeptide within the (a) L-Arg-L-Xaa; (b) L-Arg-D-Xaa; (c) L-Ala-L-Xaa; (d) L-Trp-L-Xaa; (e) L-Met-L-Xaa; and (f) D-Leu-L-Xaa dipeptide libraries. All L-amino acids are shaded in grey except for L-Asp (*red*). The D-amino acids are shaded in yellow except for D-Asp (*blue*).

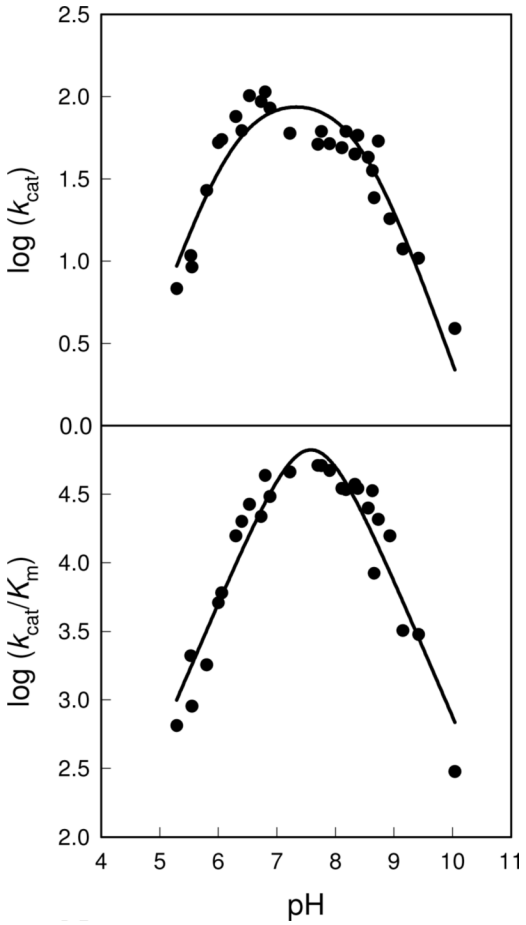

Figure 4.

pH-rate profiles for the zinc bound forms of Sco3058 using L-Arg-L-Asp as the substrate. (a) The effect of pH on k_{cat} and (b) the effect of pH on k_{cat}/K_m. Additional details are found in the text.

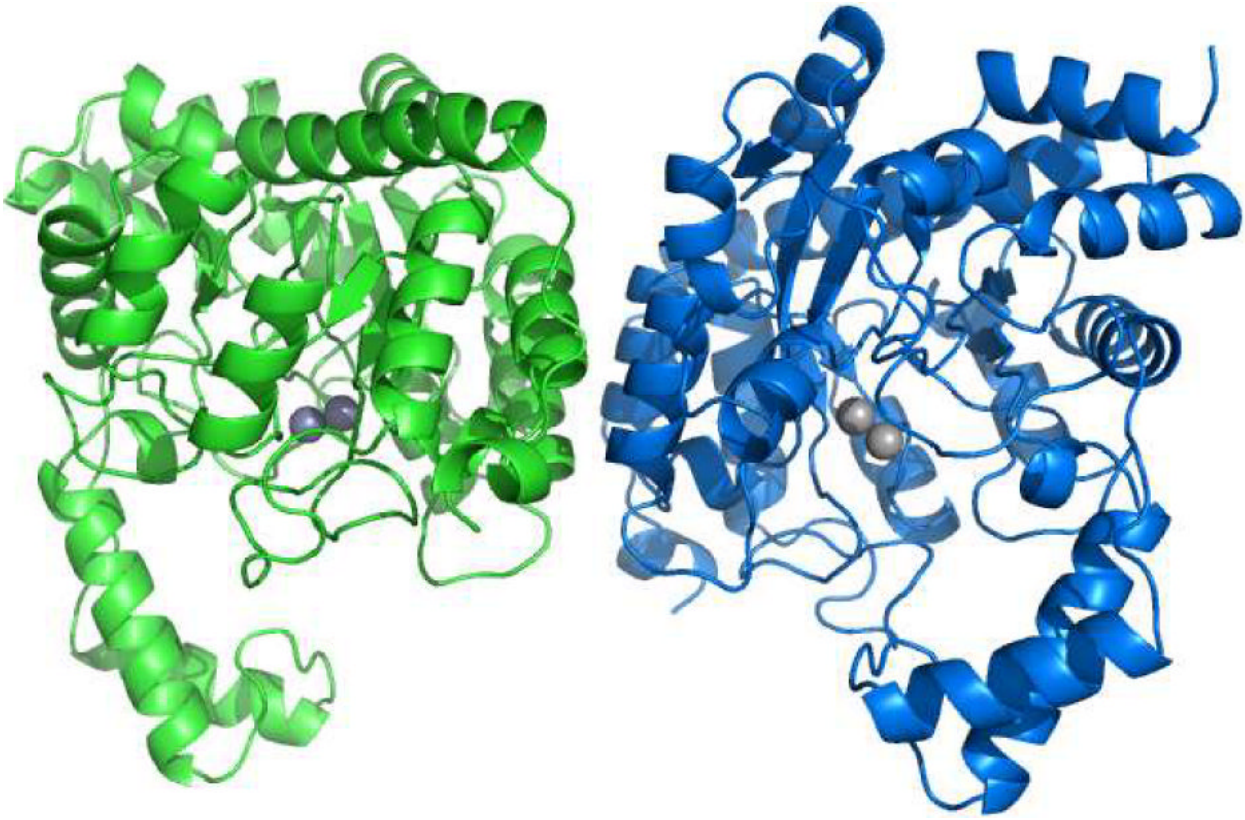

Figure 5.
Ribbon diagram of the structure of Sco3058. The two subunits are colored *green* and and *blue*. The active site metals are shown in *grey*.

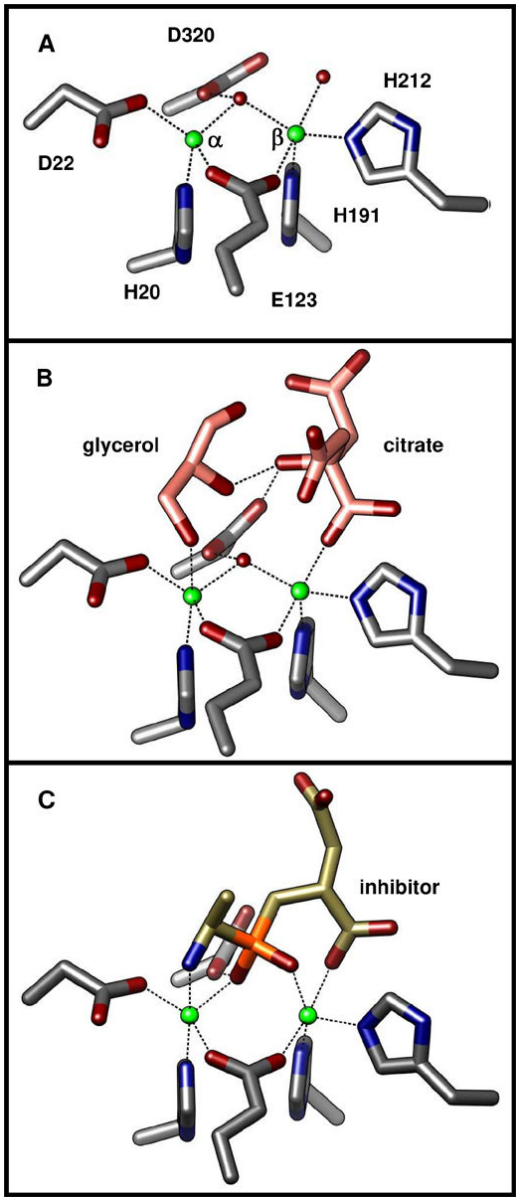

Figure 6.
Binuclear metal center of Sco3058. (a) Contacts between the zinc ions (*green* spheres) and water (*red* sphere) or active site residues are indicated with dashed lines. (b) Structure of the binuclear metal center with citrate and glycerol in the active site. (c) Structure of the binuclear metal center with the phosphinate pseudodipeptide (**1**) bound in the active site.

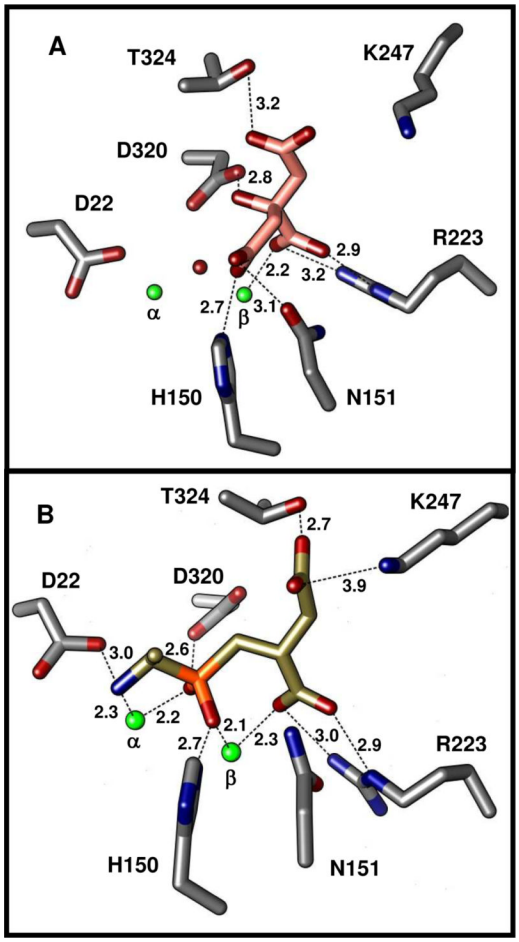

Figure 7.

Interactions of citrate and the pseudodipeptide inhibitor (**1**) bound in the active site of Sco3058. **a)** Polar contacts between citrate (*salmon* carbons) bound in the active site of Sco3058 (*grey* carbons). **b)** Polar contacts between inhibitor (**1**) (*gold* carbons and *orange* phosphorus) and Sco3058 (*grey* carbons). Polar contacts are indicated with dashed lines with distances displayed in Å. The zincs and bound water molecule are represented as *green* and *red* spheres, respectively.

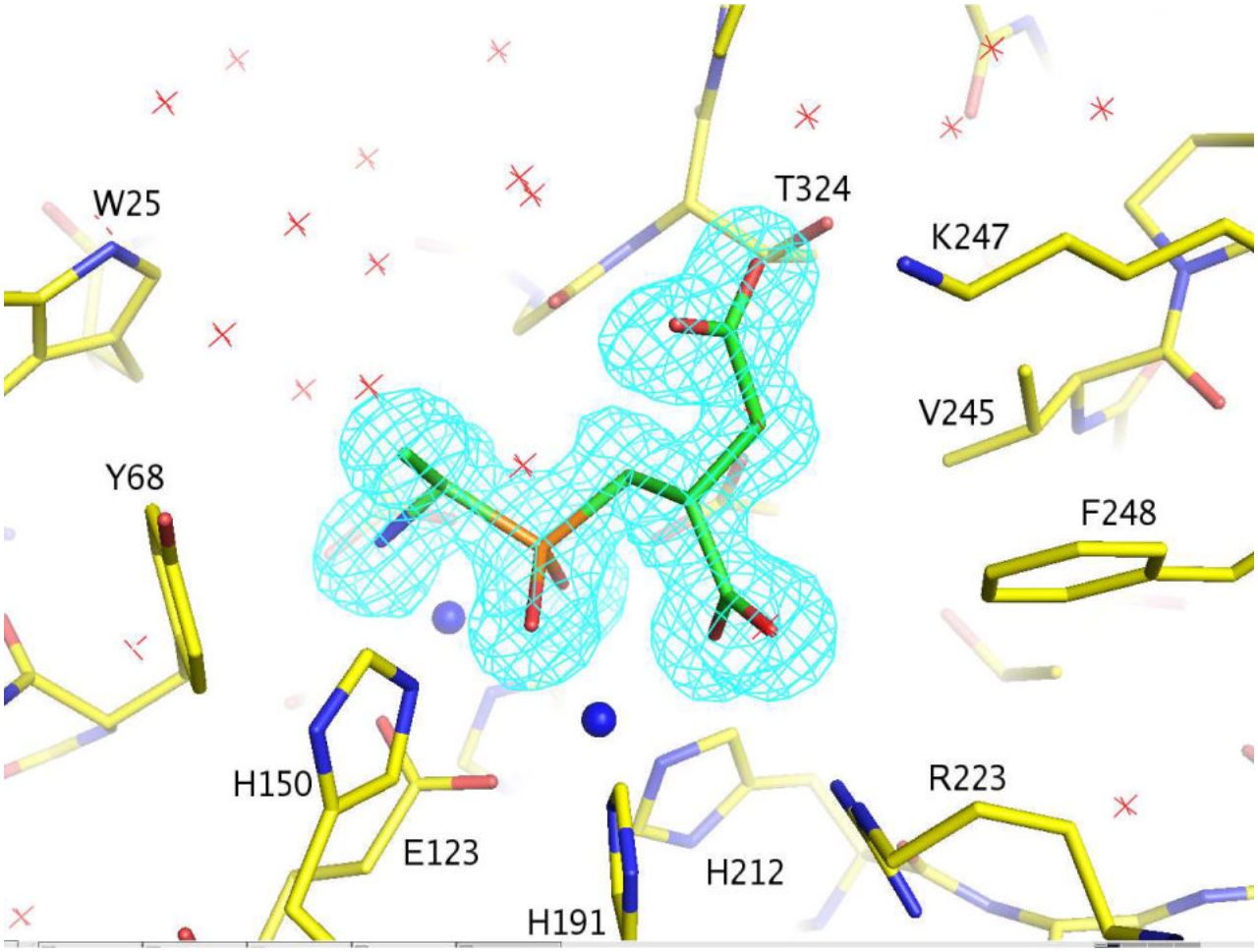

Figure 8.

Representative electron density for L-Ala-D-Asp pseudodipeptide (**1**) bound in active site of Sco3058. The electron density was obtained from $F_o - F_c$ omit map contoured at 4σ. The ligand was omitted from the model, and the remainder of the unit cell was subjected to a cycle of simulated annealing with CNS at 4000 °C. The details of the interactions between the pseudodipeptide and the active site are described in the text.

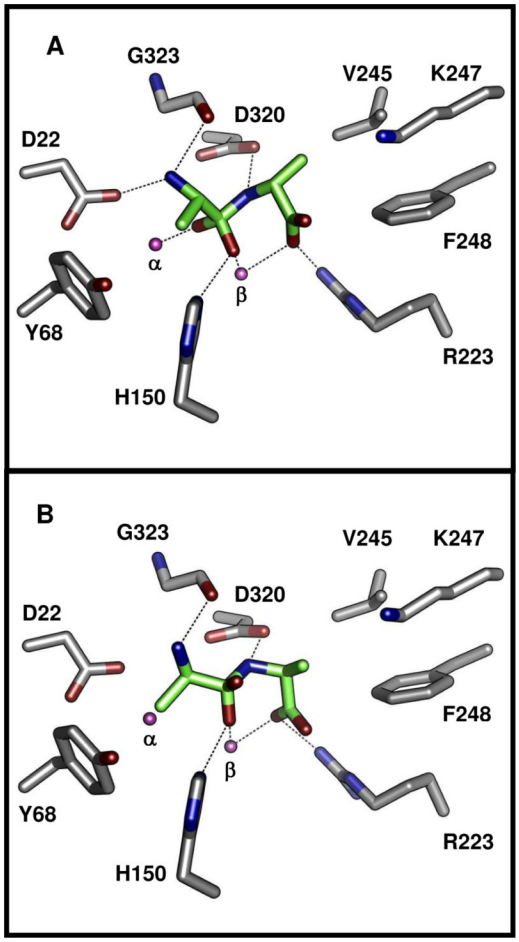

Figure 9.

Cartoon of the computed binding modes of L-Ala-D-Ala (panel a) and D-Ala-L-Ala (panel b). In both panels, the protein is depicted with *grey* carbons and the dipeptide with *green* carbons. The Zn ions, nitrogens and oxygens are colored *purple* (spheres), *blue* and *red*, respectively. All contacts between 2.1 and 3.7 Å are indicated as dashed lines.

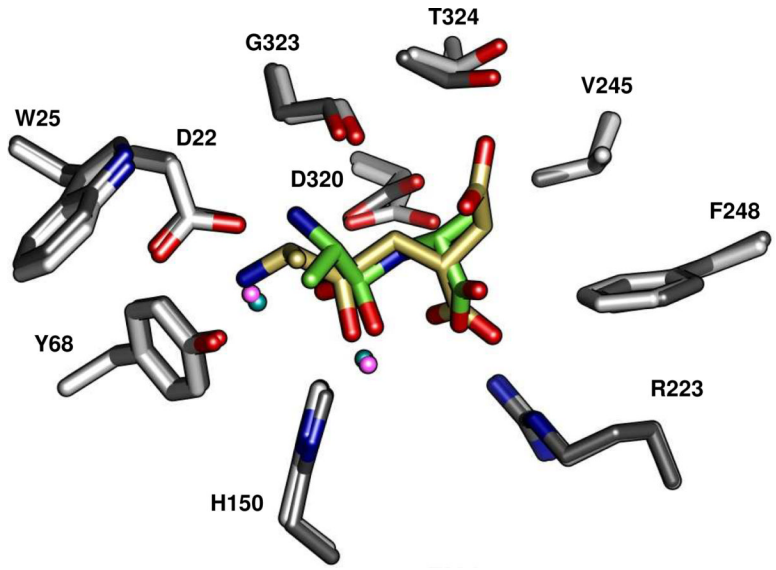

Figure 10.
Overlay of the active sites of the L-Ala-D-Asp pseudodipeptide-bound Sco3058 (*dark grey* carbons, *pink* Zn and gold inhibitor carbons) and the docked L-Ala-D-Ala-Sco3058 complex (*light grey* carbons, *teal* Zn, and *green* substrate carbons).

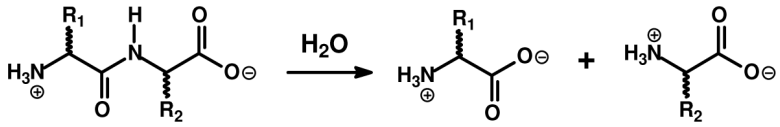

Scheme 1.

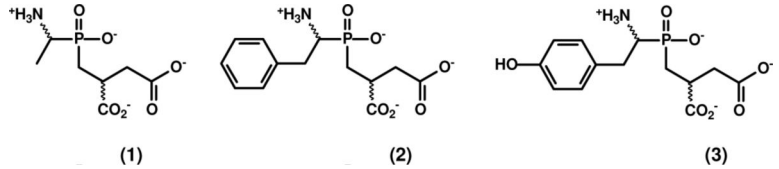

Scheme 2.

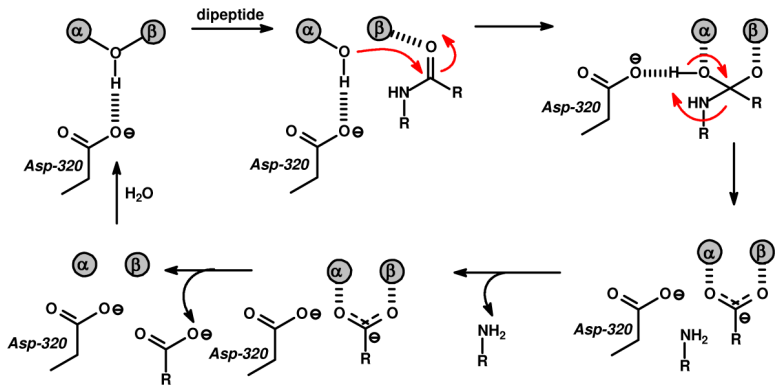

Scheme 3.

Table 1

Crystallographic statistics for Sco3058

	Sco3058	Sco3058-citrate	Sco3058-inhibitor 1
Data collection			
Beamline	NSLS X4A	SSRL 7-1	NSLS X4A
wavelength	0.97915		0.97915
space group	$P3_121$	$P3_121$	$P3_121$
# of mol. in asym.	1	1	1
Cell dimensions			
a, b, c (Å)	96.75, 96.75, 104.72	97.29, 97.29, 104.41	96.91, 96.91, 104.19
α, β, γ (°)	90.0, 90.0, 120.0	90.0, 90.0, 120.0	90.0, 90.0, 120.0
Resolution (Å)[a,b]	25–1.3 (1.35–1.30)	1.7	25–1.4 (1.45–1.40)
# of unique	133376 (9677)	62182	106229 (7419)
R_{merge}[a]	0.067 (0.449)	0.071	0.072 (0.430)
I/σ[a]	35.6 (4.2)	29.7 (4.5)	28.8 (3.8)
Completeness (%)[a]	95.9 (74.1)	98.3 (95.7)	95.3 (70.9)
Refinement			
Resolution (Å)[a]	25.0–1.3	20.0–1.7	25.0–1.4
R_{cryst}	0.184	16.7	0.193
R_{free}	0.198	20.3	0.206
Protein atoms	2980	3055	2980
Waters	390	504	417
Rmsd, bond lengths	0.004	0.018	0.004
Rmsd, bond angles (°)	1.3	2.4	1.3
Bound inhibitor		citrate, glycerol	L-Ala-D-Asp pseudodipeptide
Inhibitor atoms		19	15
Bound ions	2 Zn^{2+}	2 Zn^{2+}	2 Zn^{2+}
PDB entry	3ID7	3ITC	3K5X

[a] ASU, asymmetric unit

[b] Numbers in parentheses indicate values for the highest resolution shell.

Table 2

Kinetic constants for select substrates of Sco3058[a]

Substrate	k_{cat}, s^{-1}	K_m, mM	k_{cat}/K_m M^{-1} s^{-1}
L-Arg-D-Asp	107 ± 3.2	0.14 ± 0.02	(7.6 ± 0.9) × 10^5
L-Met-D-Glu	340 ± 4	0.89 ± 0.04	(3.8 ± 0.2) × 10^5
L-Met-D-Leu	194 ± 4	0.56 ± 0.03	(3.5 ± 0.3) × 10^5
L-Leu-D-Glu	135 ± 2	0.55 ± 0.03	(2.5 ± 0.1) × 10^5
L-Leu-D-Ala	160 ± 3	0.75 ± 0.04	(2.1 ± 0.1) × 10^5
L-Leu-D-Ser	400 ± 10	2.0 ± 0.2	(2.0 ± 0.1) × 10^5
L-Ala-D-Ala	750 ± 25	4.4 ± 0.3	(1.7 ± 0.1) × 10^5
L-Tyr-D-Leu	24 ± 0.2	0.17 ± 0.01	(1.5 ± 0.07) × 10^5
L-Met-L-Leu	310 ± 6	2.3 ± 0.1	(1.4 ± 0.1) × 10^5
L-Asn-D-Glu	288 ± 10	2.4 ± 0.2	(1.2 ± 0.1) × 10^5
L-Ala-L-Asp	1400 ± 60	13.8 ± 0.9	(1.0 ± 0.1) × 10^5
L-Leu-L-Leu	140 ± 6	1.4 ± 0.1	(1.0 ± 0.1) × 10^5
L-Leu-L-Asp	160 ± 11	2.0 ± 0.3	(8.3 ± 1.4) × 10^4
L-Arg-L-Asp	132 ± 2	1.8 ± 0.1	(7.2 ± 0.4) × 10^4
L-Leu-D-Leu	21 ± 0.3	0.37 ± 0.03	(5.6 ± 0.4) × 10^4
Gly-D-Leu			(3.3 ± 0.1) × 10^4
L-Ala-L-Glu	220 ± 14	9.5 ± 1.0	(2.4 ± 0.3) × 10^4
L-Arg-Gly			(2.2 ± 0.1) × 10^4
L-Ala-L-Ala			(1.4 ± 0.04) × 10^4
L-Ala-L-Gln	140 ± 17	16 ± 3.3	(8.4 ± 1.9) × 10^3
L-Ala-L-His			(4.5 ± 0.1) × 10^2
L-Ala-L-Arg			(1.8 ± 0.1) × 10^2
D-Ala-D-Ala			(1.3 ± 0.05) × 10^2
L-Ala-L-Lys			(7.2 ± 0.2) × 10^1
D-Ala-L-Ala			(2.2 ± 0.05) × 10^0

[a]From fits of the data to equation 2. For those entries without values of k_{cat} and K_m, saturation was not achieved at concentrations up to 5 mM.

Table 3

Kinetic parameters for mutants of Sco3058[a]

Enzyme	k_{cat} (s^{-1})	K_m (mM)	k_{cat}/K_m (M^{-1} s^{-1})
WT	132 ± 2	1.8 ± 0.1	(7.2 ± 0.4) × 10^4
D22H	<0.03		
H150N	0.7 ± 0.01	4.9 ± 2.1	(1.4 ± 0.4) × 10^2
H150A	7.2 ± 0.4	4.3 ± 0.5	(1.7 ± 0.2) × 10^3
R223K	0.4 ± 0.04	8.8 ± 1.4	46 ± 9
R223M	<0.03		
D320N	<0.03		
D320A	<0.03		

[a]These constants were obtained by a fit of the data to equation 2.